

*LIGO Laboratory / LIGO Scientific Collaboration*

LIGO- T1300595-v1

*aLIGO*


---

## Estimate of thermal and seismic noise from aLIGO quad suspension blade springs

---

Liam Cunningham, Mark Barton, Giles Hammond, Norna Robertson, Ken Strain,  
Calum Torrie

Distribution of this document:  
LIGO Scientific Collaboration

This is an internal working note  
of the LIGO Laboratory.

**California Institute of Technology****LIGO Project – MS 18-34****1200 E. California B****Pasadena, CA 911**

Phone (626) 395-21

Fax (626) 304-983

E-mail: info@ligo.caltech

**LIGO Hanford Observ****P.O. Box 159****Richland WA 9935**

Phone 509-372-8106

Fax 509-372-8137

**Massachusetts Institute of****Technology****77 St – NW22-295****Cambridge, MA 02139**

Phone (617) 253-4824

Fax (617) 253-7014

E-mail: info@ligo.mit.edu

**LIGO Livingston Observatory****P.O. Box 940****Buena Vista, LA 70754**

Phone 225-686-3100

Fax 225-686-7189

**Institute for Gravitational  
Research****University of Glasgow****Kelvin Building****Glasgow G12 8QQ**

Phone: +44 (0)141 330 3340

Fax: +44 (0)141 330 6833

Web:

[www.phvsics.gla.ac.uk/iagr/](http://www.phvsics.gla.ac.uk/iagr/)<http://www.ligo.caltech.edu/>

## Abstract

This document provides a brief overview of the calculation of the displacement noise observed at the test mass of an aLIGO quadruple pendulum suspension caused by excitation of the maraging steel blade springs.

There are two sources of this displacement noise. The first is from the undamped seismic excitation of the suspension which is a motion of the entire payload this excites the internal modes of the blade springs and this can then be transmitted to the test mass. The other noise source of interest here is the thermal excitation of the internal resonances of the cantilever blade springs on the upper intermediate mass which can then be transmitted to the test mass.

## Introduction

This document is an update to earlier calculations of seismic and thermal noise from the aLIGO quad which can be expected to be transmitted to the test mass, DCC T050046<sup>[1]</sup> the calculations from which are included in Appendix A. An estimate for the seismic noise is calculated by using ANSYS FEA software to model the full quad pendulum consisting of 3 levels of metal blade spring/ wires and 1 monolithic silica stage. The transmissibility of this is used to estimate how much noise is transmitted.

The thermal noise originating from the cantilever springs on the upper intermediate mass of the quad pendulum is then modelled independently. Three different approaches are taken which give comparable thermal noise performance. A suitable transmissibility is calculated and the thermal noise due to excitation of the lower blades is calculated.

## 1 Seismic noise

The calculation of the seismic noise transmitted to the test mass required modeling of the full aLIGO quad suspension. The residual noise at the top of the chain is filtered by successive pendulum stages

The aLIGO quad model, D0901346, was stripped back to just the blades and immediate supporting structure as shown below in Fig1.

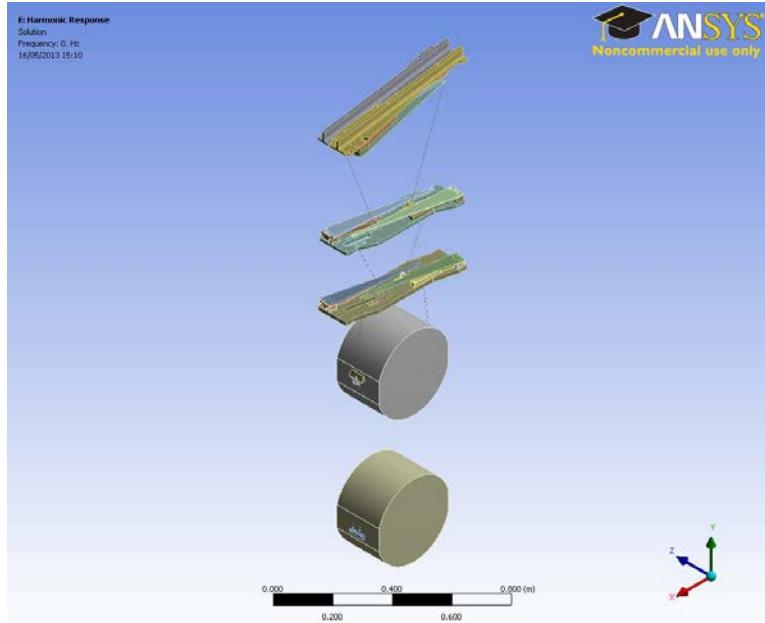


**Figure 1 aLIGO quad structure stripped down for analysis**

The model has flat profile blades modeled as real solids but without a pre-stress. The metal wires and glass fibers were replaced with appropriately dimensioned stiff beams to remove the large number of violin like modes that occur due to the lack of tension. The structural modes were calculated and then a harmonic analysis performed to get the motion of the blades and test mass at the resonances of the 3 blades. The motion of the system at each of the three resonances are shown in Figures 2-4. The loss values used for the harmonic analysis are shown in Table 1.

**Table 1 loss angle for materials used in the simulation**

<b>Material</b>	<b>Loss angle <math>\phi</math></b>
Silica (test mass)	$3.8 \times 10^{-8}$
Silica (fibre)	$1.6 \times 10^{-9}$ [2]
Maraging steel	$1 \times 10^{-4}$
Stainless steel	$1 \times 10^{-3}$

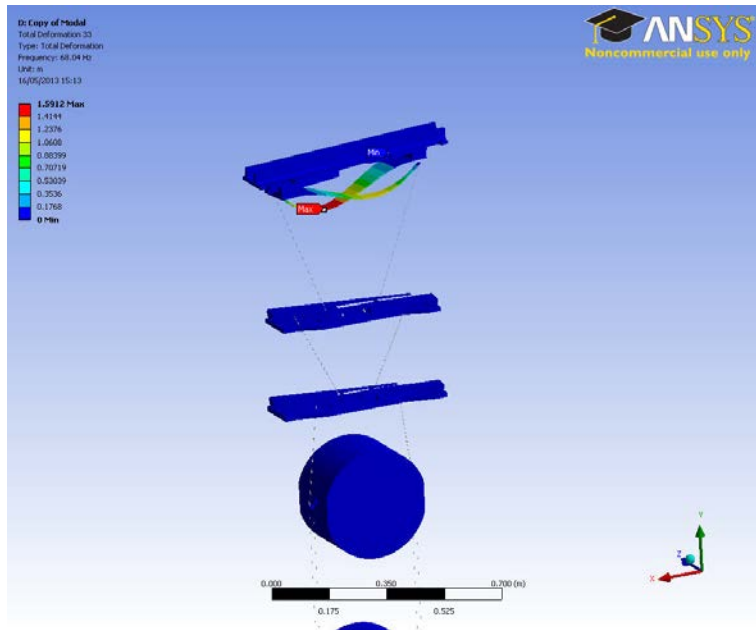


Figure 2 Motion of top blades at 68 Hz resonance

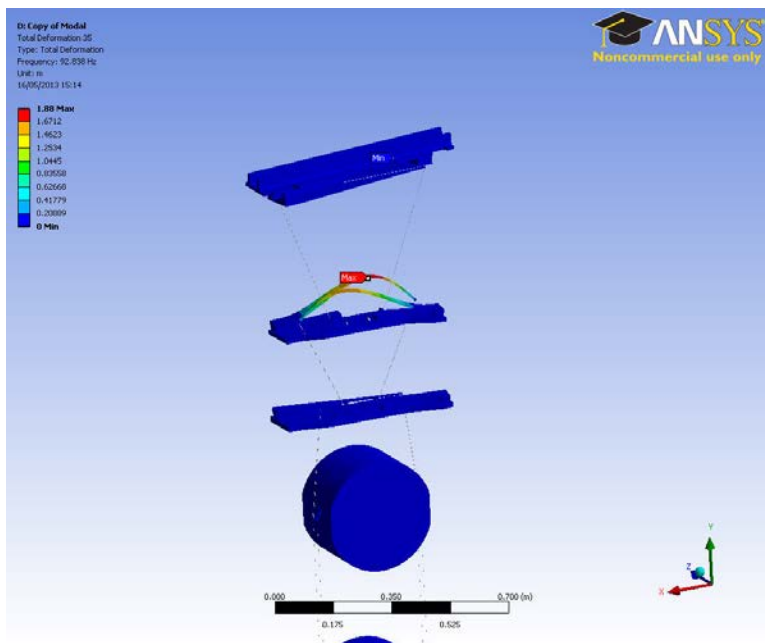


Figure 3 Motion of middle blades at 93 Hz resonance

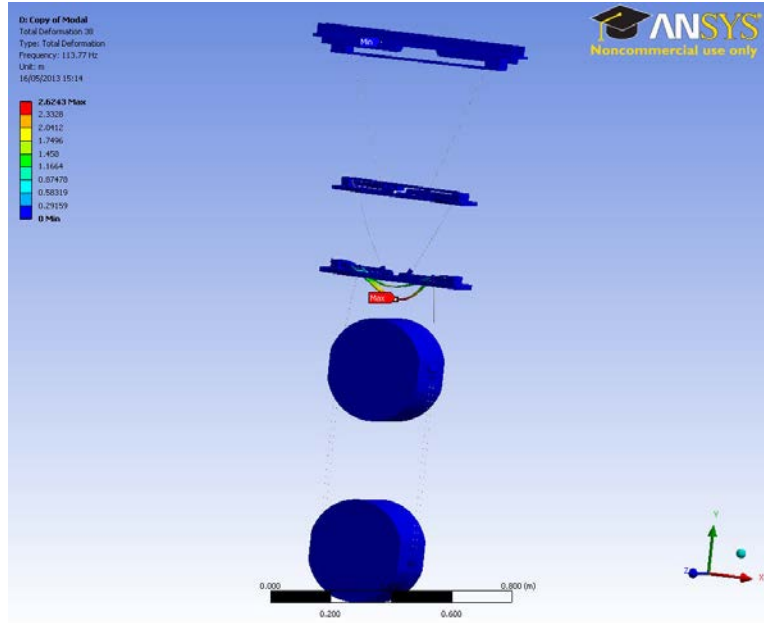


Figure 4 Motion of bottom blades at 113 Hz resonance

The combined transmissibility has been plotted in Figure 5 below. Around the resonance the values go in 1 mHz steps to improve resolution. The transmissibility measured here is for a vertical excitation applied to the support structure of the upper blades and the vertical motion is observed at the test mass.

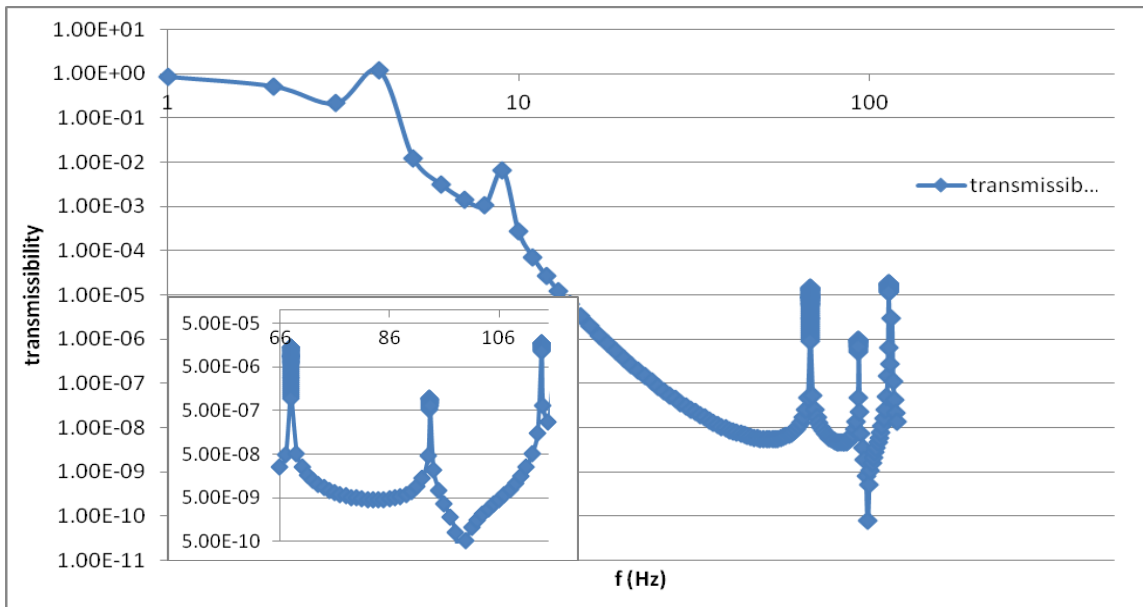


Figure 5 Transmissibility of full quad suspension. The upper stage is vertically excited and the motion is measured at the test mass. Inset shows close up of peaks.

The transmissibility measured for each of the three resonances is  $1.44 \times 10^{-5}$  at 68.014 Hz (top blade resonance)  $9.66 \times 10^{-7}$  at 93.357 Hz (middle blade resonance) and  $1.78 \times 10^{-5}$  at 113.780 Hz (lower blade resonance) Using this to calculate the residual seismic noise gives the results in Table 2. The longitudinal noise per test mass, col. 6, is given by multiplying cols. 3-5 together. The seismic residual noise in column 5 is a requirement of the seismic isolation system as detailed in LIGO E990303<sup>[3]</sup>

**Table 2 Residual seismic noise at each of the three resonances calculated from the transmissibility of a full quadruple suspension with unstressed blades and rigid wires.**

				seismic	longitudinal noise	target strain	target sensitivity	factor
		transmissibility	cross-coupling	residual	test mass	sensitivity	per test mass	below
Blade	1st int (Hz)	at resonance		(m/rtHz)	(m/rtHz)	(1/rtHz)	(m/rtHz)	target
Top	68.014	1.44E-05	1.00E-03	3.00E-14	4.32E-22	4.00E-24	8.00E-21	1.85E+01
Middle	93.357	9.66E-07	1.00E-03	3.00E-14	2.90E-23	3.00E-24	6.00E-21	2.07E+02
Bottom	113.78	1.78E-05	1.00E-03	3.00E-14	5.34E-22	2.50E-24	5.00E-21	9.36E+00

The excess seismic noise transmitted to the test mass at the first internal modes of each of the 3 stages of blade springs has been calculated to have a minimum factor of safety of 9 below the target sensitivity. This compares well with the desired noise levels given in T010075-01<sup>[4]</sup> which recommends that technical noise sources are a factor 10 below the desired sensitivity.

The transmitted noise observed here is lower than that reported in T050046 this can be explained by a number of factors. The original work used a transmissibility for each single blade, having a simple trapezoidal shape, and multiplied to get the combined transmissibility of the three stages, see T040061<sup>[6]</sup>. This current work uses the blade shapes for the aLIGO production blades, as an example the lowest blade, D060327 is shown in Figure 6, and is modelling a full suspension system of 3 metal stages and 1 monolithic stage. This allows for coupling between the modes of the suspended components. It should also be noted that the original work used a Q of  $2 \times 10^4$  for the maraging steel blades rather than the  $10^4$  used in the current work.

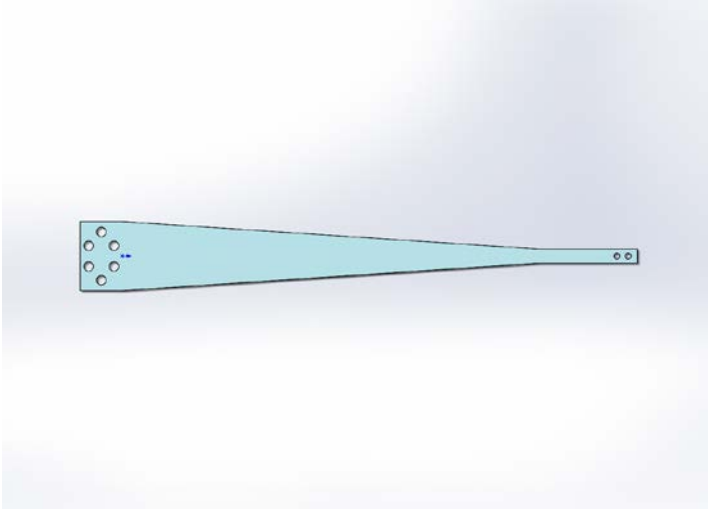


Figure 3 D060327 Lower blade for aLIGO quad suspension

The low level of transmitted noise means that it should not be necessary to apply damping to the blades due seismic excitation of the resonant modes of the maraging steel blade springs.

## 2 Thermal noise

Thermal noise can be transmitted to the ITM/ ETM due to excitation of the internal modes of the lowest set of metal blade springs. There are 3 methods used to calculate the possible levels of the thermal noise and each require a different analysis of the transmissibility of the lower stages of the quad suspension.

### 2.1 RMS displacement

This approach follows the derivation outlined in Ref [1], where it is assumed that the *rms* displacement is related to the thermal energy via

$$m\ddot{x}x = k_B T \quad (1)$$

with  $m$  as the mass of the oscillating spring, and  $\ddot{x}, x$  are the acceleration and displacement respectively. Assuming a harmonic response, gives an *rms* displacement

$$x^2 = \frac{k_B T}{4\pi^2 m f_0^2} \quad (2)$$

If it is assumed that the Quality factor is  $Q = 1/\phi$  with resonant frequency  $f_0$ , then the bandwidth can be written as  $\Delta f = \frac{f_0}{Q}$ , which gives an amplitude spectral density of

$$x = \sqrt{\frac{k_B T Q}{m 4\pi^2 f_0^3}} \quad (3)$$

For the 1<sup>st</sup> internal mode of an aLIGO upper intermediate mass  $Q = 10^4$ ,  $m = 0.36 \text{ kg}$ ,  $f_0 = 113.78 \text{ Hz}$ , which results in a spectral density of  $x = 1.4 \times 10^{-12} \text{ m}/\sqrt{\text{Hz}}$  at resonance.

## 2.2 Fluctuation dissipation theorem (FTD)

The amplitude spectral density as a function of frequency can be obtained via direct application of the fluctuation dissipation theorem. The amplitude spectral density is related to the real part of the admittance,  $Y$ , via

$$x^2 = \frac{4k_B T}{4\pi^2 f^2} \Re[Y] \quad (4)$$

which can be written as

$$x^2 = \frac{k_B T}{2m\pi^3 f} \left( \frac{f_0^2 \phi(\omega)}{f_0^4 \phi^2(\omega) + (f_0^2 - f^2)^2} \right) \quad (5)$$

For the 1<sup>st</sup> internal mode of an aLIGO upper intermediate mass spring,  $\phi = 1/Q = 10^{-4}$ ,  $m = 0.36 \text{ kg}$ ,  $f_0 = 113.78 \text{ Hz}$ , and this results in an amplitude spectral density of  $x = 1.2 \times 10^{-12} \text{ m}/\sqrt{\text{Hz}}$  at resonance. Figure 7 shows the amplitude spectral density as a function of frequency. The green dot at the resonance is the value obtained from the *rms* approach described above.



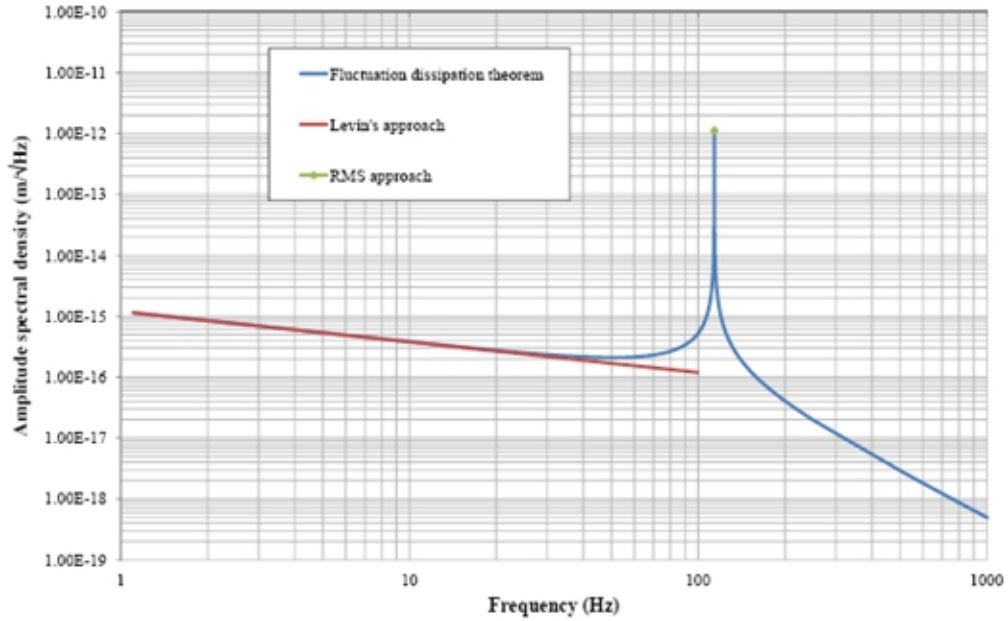


Figure 4 Comparison of the three methods to calculate the amplitude spectral density of the cantilever spring thermal noise.

### 2.3 Levin’s direct approach

The final method which can be applied to calculate the thermal noise is the approach of Levin<sup>[5]</sup>. In this case a notional force (1N in this case) is applied at the centre of a blade spring fixed at both ends to mimic the motion of the internal mode to derive the strain energy when the blade undergoes oscillations in the 1<sup>st</sup> internal mode. The deformation of the blade is shown in Figure 8.

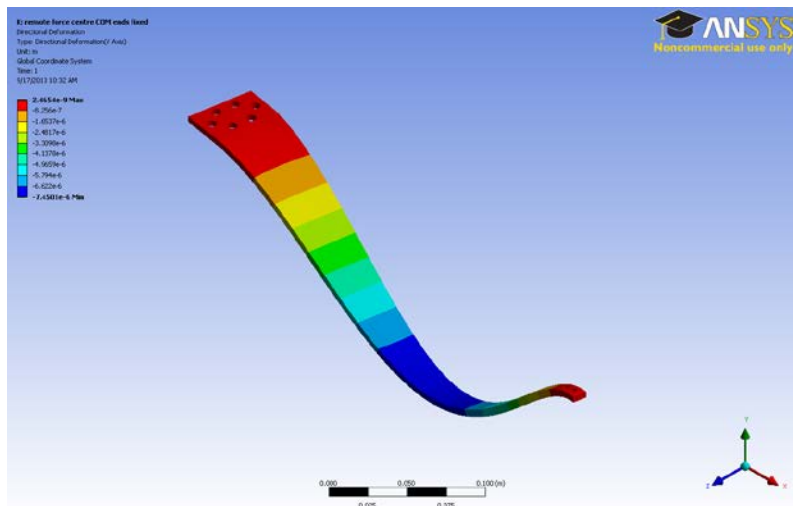


Figure 5 Deformation of lower blade caused by a 1N force acting on the centre of motion.

The dissipated power is given by

$$W_{diss} = 2\pi f \phi \varepsilon \quad (6)$$

with strain energy  $\varepsilon$  which is readily derived from the FEA model. For the case of the aLIGO upper intermediate mass spring  $\varepsilon = 2.7 \times 10^{-6}$  for a 1N force applied at the blade spring centre. The off resonance amplitude spectral density is then

$$x^2 = \frac{2k_B T}{m\pi f} \frac{W_{diss}}{F_0} \quad (7)$$

with a notional force  $F_0$ . Figure 7 above also shows a plot of the frequency dependence of the amplitude spectral density. It is important to note that this approach does not predict the on-resonance thermal noise. This is consistent with previous applications of the Levin method e.g the thermal noise of a finite size mirror well below the internal resonant modes.

The FDT method and Levin's method give identical off-resonance thermal noise estimates. Furthermore, the *rms* approach and the fluctuation dissipation theorem give on resonance amplitude spectral densities which are similar to 10%. Levin's method only provides an estimate for the thermal noise at frequencies below the resonance of the mode which is being modelled as it does not have a mechanism for including the resonance of the blades. This is identical to the approach taken with the finite size LIGO mirrors and mirror thermal noise terms due to the operation frequency being several kHz below the resonant modes of the test mass

## 2.4 Transmissibility of blades

In order to calculate the thermal noise sensed at the test mass it is essential to have the correct transmissibility of the system. The RMS and FTD methods both take into consideration that the system is at resonance as shown in Figure 7 above while the Levin method does not, so this requires two different methods to calculate the transmissibility.

### 2.4.1 Transmissibility for RMS/ FTD Approaches

The transmissibility for these methods relies on treating the blade springs as rigid bodies. This means that the blade response spectrum is treated as if the internal mode resonance does not exist. To get the approximate transmissibility of a rigid blade the first stage is to model a single blade with a realistic metal wire with a 19.6 kg load attached to simulate half of a PUM. The blue curve in Figure 9

shows the transmissibility of this system. The blade is vertically excited at the root and the motion measured at the end of the wire. The peak at ~330 Hz is associated with the wire.

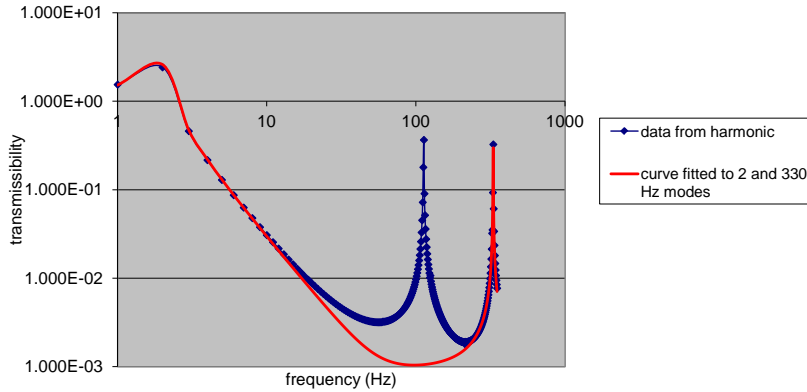


**Figure 6 Response spectrum from single lower blade with 19.6 Kg on end of a real wire. The blade is excited at the root and the motion is measured at the end of the wire**

The curve is then fitted using a combination of  $1/(1-(f/f_0)^2)^2$  curves for the first and third resonances to remove the resonance at 113 Hz. This is shown by the red curve in Figure 9. This is used to make an estimate of the transmissibility at the resonant frequency. In Figure 9 it is 0.00106. The displacement spectrum is also measured for the monolithic section of the suspension at the resonant frequency. These are then combined to give the transmissibility for the whole lower section of the system.

The combined system of the blade with wire/ monolithic structure has a combined transmissibility of  $2.9 \times 10^{-6}$ . Using the thermal noise value calculated above for the single blade thermal noise at the resonance of 113 Hz the thermal noise transmitted to the test mass is given by

$$x_{test\ mass} = x_{blade} \times trans_{combined} \times cross\ coupling\ factor \times \sqrt{2} \quad (8)$$

Where the *cross coupling factor* is  $1 \times 10^{-3}$  and the  $\sqrt{2}$  is because of the two blades. This gives a thermal noise of  $5.7 \times 10^{-21}$  m/ $\sqrt{\text{Hz}}$ . This is approximately equal to the target sensitivity per test mass at 100 Hz in aLIGO<sup>[2]</sup> and is an improvement by ~ factor of three over previous estimates<sup>[1]</sup>, again this is caused by the change in the shape of the blades. However, this noise level is still a factor of ~10 above the desired value of  $\sim 5 \times 10^{-22}$  m/ $\sqrt{\text{Hz}}$ .

## 2.4.2 Transmissibility of blades for Levin's method

As noted above, Levin's method provides a good estimate for the off-resonance case but fails to correctly predict the increase in thermal noise at resonance as seen in the RMS and FDT cases. This method, if used with the same transmissibility value as above would result in a much lower value of the thermal noise than may be expected. In this instance the transmissibility of the lower stages of the quad suspension were modelled independently and the transmissibility for the combined system used to calculate the thermal noise transmitted to the test mass from thermal excitation of the lower blades. Figure 10 shows the UIM+ Monolithic subsystem to be modelled.

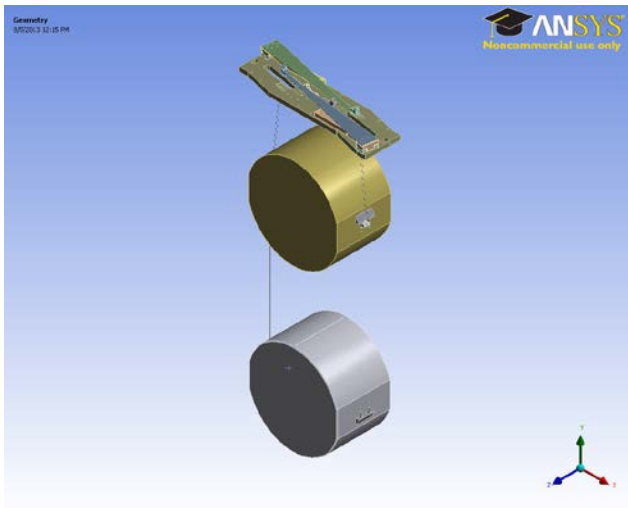


**Figure 7 UIM and monolithic section of aLIGO quad. Blades are flat profile, wires and fibres are realistic elements.**

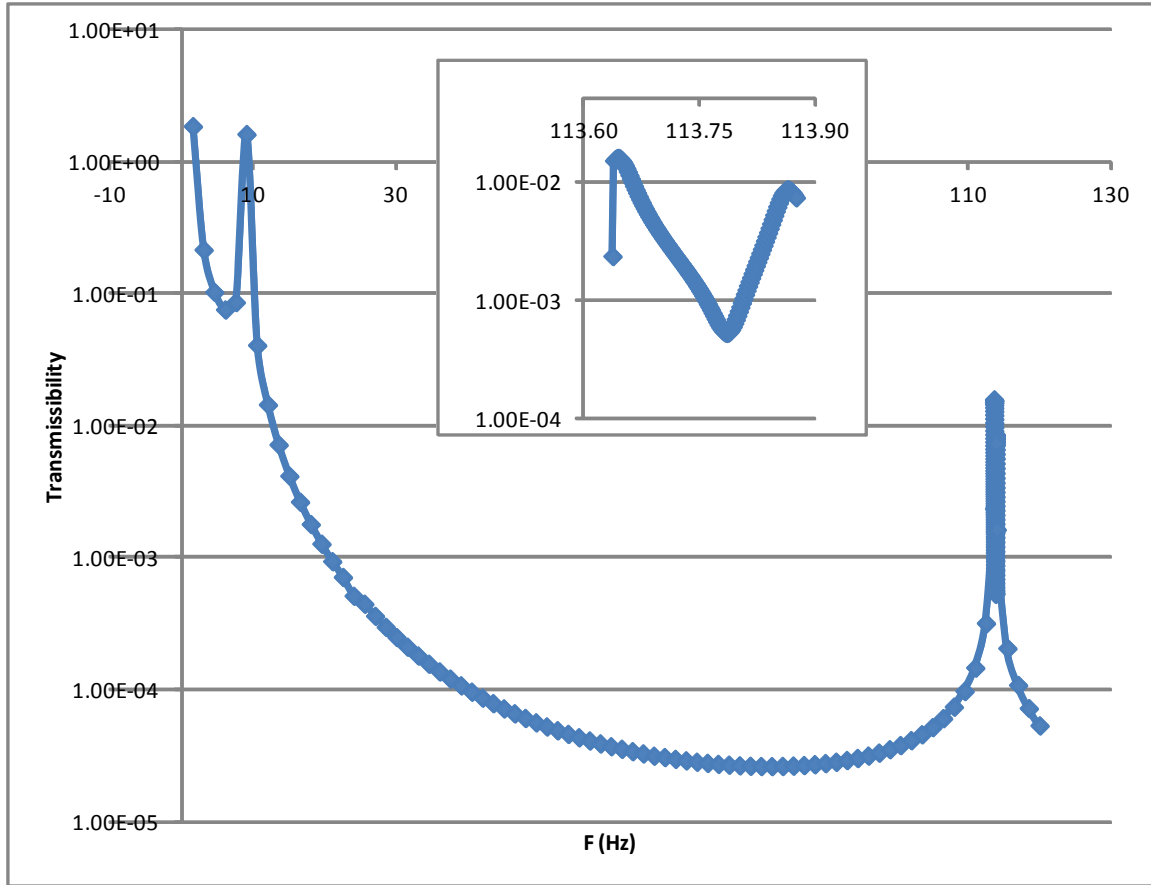


Figure 8 Response spectrum measured at the test mass when the UIM is excited vertically. Insert shows two peaks; one for each blade separated by 0.2 Hz.

The transmissibility curve, shown in Figure 11, for this system was taken from the vertical movement of the test mass, giving a value of 0.015 at the resonance frequency of  $\sim 113$  Hz. The thermal noise transmitted to the test mass can then be calculated using Eq. 8. This gives a thermal noise value of  $2.3 \times 10^{-21}$  m/ $\sqrt{\text{Hz}}$  at the test mass. This value is still  $\sim 5$  times greater than the desired level but is lower than that calculated using the RMS and FDT methods. The comparison between the different methods is shown in Table 3.

Table 1 Comparison of transmitted thermal noise measured at the test mass calculated using three different methods

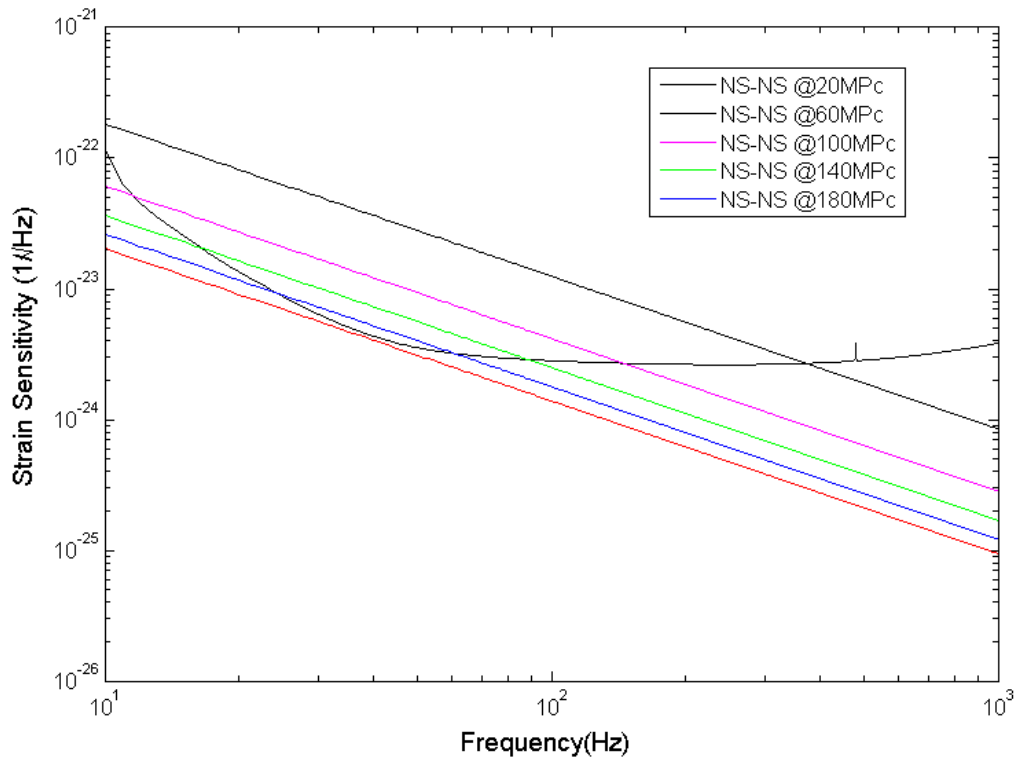
Method	Thermal noise per blade ( $x_{blade}$ ) (m/ $\sqrt{\text{Hz}}$ )	Transmissibility ( $trans_{combined}$ )	Thermal noise at test mass ( $x_{testmass}$ ) (m/ $\sqrt{\text{Hz}}$ )
FDT	$1.2 \times 10^{-12}$	$2.9 \times 10^{-6}$	$5.7 \times 10^{-21}$
RMS	$1.4 \times 10^{-12}$	$2.9 \times 10^{-6}$	$5.7 \times 10^{-21}$
Levin	$1.1 \times 10^{-16}$	0.015	$2.3 \times 10^{-21}$

Figure 11 also shows that there are separate peaks for each blade. The peaks at the blade resonances here are very narrow with a total width for the two resonances of  $\sim 0.3\text{Hz}$ . Each individual peak has a width of less than  $0.1\text{ Hz}$ . This offsetting is due to minor differences in the mesh of the two blades leading to very small differences in the mass distribution. By careful matching of the blades so that the resonances are the same this problem would be alleviated. The blade matching documented in T1000068-v2 suggests a difference in loaded height between pairs of blades of  $0.2\text{mm}$  or less. This equates to a  $0.125\%$  difference in blade stiffness and would suggest a frequency separation between pairs of blades of at most  $0.04\text{ Hz}$  at the  $113\text{Hz}$  resonance. However, to take into consideration any inconsistencies in the assembly of the blade subsystems a width of  $0.3\text{ Hz}$  seems a reasonable conservative estimate.

This suggests that the use of damping may not be necessary if the detector readout can be filtered in a  $0.3\text{ Hz}$  bandwidth at the resonant frequency of the blades. Assuming the distribution shown in Figure 11 the transmissibility has dropped by at least a factor 3 at  $50\text{mHz}$  from the peak, this would lead to a thermal noise level three times lower which is approaching the desired level of sensitivity of  $\sim 5 \times 10^{-22}\text{ m}/\sqrt{\text{Hz}}$

## Effect of notching the detector signal

The narrow bandwidth of the thermal noise signal means that it should be possible to apply a notch filter to the detector signal at the resonant frequency of the blades. To estimate how much this filter would degrade a potential detectable signal from a NS binary system a  $1.4\text{M}-1.4\text{M}$  mass binary system was modelled at a variety of distances. Figure 12 shows the aLIGO target sensitivity and the expected signals.



**Figure 9 Interaction of aLIGO target sensitivity curve with expected signal levels for NS-NS systems at varying distances**

To test a worst case scenario, the ratio of the signal with a  $\pm 1$ Hz data analysis filter applied to the un-filtered signal is shown in Table 3. This size of filter is much larger than would be required but it may be easier to setup a single filter which will cover a large range of possible blade resonances where frequency shifts may be expected due to minor inconsistencies in blade manufacture and assembly procedures.

**Table 2 Ratio of signal power with a notch filter to power without a notch filter for NS binaries over the aLIGO band.**

Distance (Mpc)	Signal power ratio (with filter/without filter)
20	0.9978
60	0.99857
100	1
140	1
180	NaN

This calculation shows that for the close binary systems, despite simulating the effect of data analysis methods weighting out a 2Hz window at ~113 Hz, there is plenty of potential power available elsewhere. This in turn means that the chances of detection are not reduced by any significant amount. For the more distant binaries; either the signal is not detected at 113 Hz, so the filter will have no effect hence the ratio of 1 above, or the furthest away sources are below the target sensitivity altogether. This calculation was performed for a single detector looking in one direction, other configurations may have slight variations but overall the effect would appear to be very small.

## Conclusions

The transmission of noise to the ITM/ ETM from excitation of the blades by residual undamped seismic activity appears to be well within acceptable limits. At the 113 Hz resonance of the lowest set of blades the seismic noise transmitted to the test mass is ~9 times lower than the target sensitivity. This gives noise levels of  $\sim 5.3 \times 10^{-22}$  m/ $\sqrt{\text{Hz}}$  which is comparable with the desired upper level for an individual technical noise source<sup>[3]</sup>. This suggests that the seismic noise is not a cause for concern and that damping is not necessary to deal with it.

For thermal noise the differences in the 3 analytical approaches requires different modelling for the transmissibility of the lower stages. When this is taken into consideration the results for the RMS/FDT method and Levin's method are within ~ a factor of 2 of each other. However, even the lower value of thermal noise calculated using Levin's method is still above the desired noise level. However, Table 3 above shows that using a noise filtering algorithm around the resonance frequency of the lower blades would have an extremely small effect on the potential for detection of NS binaries.

In conclusion, due to the low level of noise power present in the detection band we propose that it is acceptable to operate the detector without replacing the magnetic damping system. We also note that adding a non-magnetic damping system such as a tuned mass damper is non trivial due to lack of space and suitable attachment points

## Appendix A



## Seismic and thermal noise calculations taken from T050046-01

The longitudinal noise at the test mass (column 7) is calculated by multiplying the entries in columns 3, 4, 5 and 6, where the residual noise level on the seismic platform (column 6) is taken from the Seismic Design Requirements Document (E990303-03-D). The target sensitivity per test mass (column 9) is given by target sensitivity (column 8) \*2000. The final column is the ratio column9/column7.

Blade	freq of mode	peak height	transmissibility	X-coupling factor	platform residual	long. noise	target	target	factor below
	fm (Hz)	(transmissibility of blade stages)	of final stage (fo/fm)^2	(vert. to long.)	vert. noise (m/rtHz)	at test mass (m/rtHz)	sensitivity* h (1/rtHz)	sensitivity per mass (m/rtHz)	target s'tivity
top	69.4	6.45E-03	7.73E-03	1.00E-03	3.00E-14	1.50E-21	4.00E-24	8.00E-21	5.35
middle	96.6	9.32E-03	3.99E-03	1.00E-03	3.00E-14	1.12E-21	3.00E-24	6.00E-21	5.38
bottom	113.6	5.23E-03	2.88E-03	1.00E-03	3.00E-14	4.52E-22	2.50E-24	5.00E-21	11.07

The most important blades for thermal noise considerations are the lowest set, nearest to the test mass, since noise associated with the blades further up the chain is better isolated at the test mass. For this blade, we have  $m = 0.31$  kg, and  $\omega = 2\pi f_b$  where  $f_b = 114$  Hz. To calculate the amplitude spectral density we divide by the root of the bandwidth  $\Delta f$  where  $\Delta f = f_b/Q$ , and hence find, with  $Q = 10^4$ , (this has changed to  $2 \times 10^4$ )

$$x = 1.5 \times 10^{-12} \text{ m}/\sqrt{\text{Hz}}$$

The resulting displacement at the test mass is given multiplying by the vertical transmissibility of that stage\* (the transmissibility treating the blade as a rigid body), the vertical transmissibility of the final stage on its silica suspension and the cross-coupling factor between vertical and horizontal, giving

$$x_{\text{from one blade}} = 1.5 \times 10^{-12} \times 3 \times 10^{-3} \times (6.1/114)^2 \times 10^{-3} = 1.3 \times 10^{-20} \text{ m}/\sqrt{\text{Hz}}$$

We should further multiply by  $\sqrt{2}$  to take account of the two blades at the lowest stage, giving

$$x_{\text{test mass}} = 1.8 \times 10^{-20} \text{ m}/\sqrt{\text{Hz}} \text{ at } 114 \text{ Hz}$$

This should be compared with a level 10 times lower than the target sensitivity per test mass at that frequency, namely  $\sim 5 \times 10^{-22} \text{ m}/\sqrt{\text{Hz}}$ .

## References

1. N. Robertson and C. Torrie, Seismic and Thermal Noise Peaks from Blade Internal Modes in an ETM/ITM Quadruple Pendulum, T050046-01, 2005
2. A V Cumming *et al* 2012 *Class. Quantum Grav.* 29 035003
3. P. Fritschel *et al* 'Seismic Isolation Subsystem Design Requirements Document' E9990303-03 2001
4. P Fritschel ed 'Advanced LIGO Systems Design', T010075-v2 2009
5. Y. Levin, Internal thermal noise in the LIGO test masses: A direct approach, *Phys. Rev. D* 57, 659–663 (1998)
6. J. Greenhalgh 'Transmissibility of a revised set of blades' T040061-01 2004